RSC Advances

ROYAL SOCIETY OF CHEMISTRY

www.rsc.org/advances

Cite this: DOI: 10.1039/c0xx00000x

www.rsc.org/xxxxxx

ARTICLE TYPE

pH-responsive near-infrared nanoprobe imaging metastases by sensing acidic microenvironment

Zhan Si[a], Cuiyun Huang[a], Xihui Gao[a] and Cong Li [a,*]

Received (in XXX, XXX) Xth XXXXXXXXX 20XX, Accepted Xth XXXXXXXXX 20XX

DOI: 10.1039/b000000x

Metastasis leads to the vast majority of cancer deaths. To reduce metastasis-associated mortality, it is crucially important to detect metastases in their early developmental stages. Due to the small volume and diffused distribution of the metastases, imaging probe to visualize the metastases with high target to background signal (T/B) ratio is prerequisite. Acidification of extracellular pH (pH_e) is a universal characteristic of solid tumor regardless of their genotypes and phenotypes. Acidic tumor microenvironment plays an important role in promoting dormant metastasis by driving protease-mediated digestion, disrupting cell-matrix interaction and increasing migration of cancer cells. Therefore, imaging tumor acidity holds the promise to visualize metastases with high sensitivity and universality. In this work, a pH responsive near-infrared (NIR) fluorescence nanoprobe **NP2** was developed, in which multiple copies of NIR fluorophores were conjugated to dextran with acid liable hydrazone bonds. Under neutral pH, the signal of the fluorophores with spatial proximity is quenched efficiently via the intramolecular electron transfer. However, the cleavage of acid liable bonds under physiologically acidic pHs with the concomitant diminishment of self-quenching effect leads to a remarkable signal enhancement. *In vivo* NIR fluorescence imaging indicated the enhanced NIR fluorescence in the chest of mouse models bearing pulmonary metastases after intravenous injection of **NP2**. *Ex vivo* fluorescence imaging demonstrated the capability of **NP2** to visualize pulmonary metastases with volumes in a range of 0.5–28 mm^3. Fluorescence microscopic imaging studies verified the high sensitivity and specificity of **NP2** to detect metastases, which was further supported by histological H&E staining. Overall, pH responsive nanoprobe **NP2** showed the feasibility to visualize the metastases with high T/B ratios by sensing the acidic microenvironment.

1. Introduction

Metastasis is an extremely complex disease that requires cancer cells to escape from the primary tumor, survive in the circulation, seed at distant sites and colonize in the secondary organ[1]. Due to the small volume, dispersal distribution nature and genetic heterogeneity of the metastases, it is very difficult to timely detect and eliminate these metastases, which results in organ failure and causes 90% of human cancer deaths[2]. Therefore, visualizing the metastases with high sensitivity and spatial resolution followed the timely treatment is crucially important to reduce the metastasis associated mortality.

Like the relationship between seed and soil[3], the metastatic behavior of tumors not only depends on their intrinsic genotypes of cancer cells (*seed*), but also closely relates to their surrounding microenvironment (*soil*)[4]. Tumor microenvironment (TME) consists of stromal cells, infiltrating immune cells, extracellular matrix (ECM), blood/lymphatic vessels and corresponding physiological conditions. Dysregulation of intratumoral pH is a universal characteristic of TME in solid tumors. In normal tissues, the intracellular pH (pH_i) and the extracellular pH (pH_e) were measured in range of 6.7–7.2 and 7.3–7.4 respectively. Solid tumors demonstrate higher pH_i values (7.3–7.6) and lower pH_e values (6.2–6.9)[5, 6]. The reversed pH gradient not only offers the evolution advantage to cancer cells[7], but also provides a niche for tumor invasion and metastasis[8]. For example, as a hallmark of TME[9, 10], acidification of tumor extracellular fluid drives protease-mediated digestion, promotes extracellular matrix (ECM) remodeling, disrupts the cancer cell-matrix interactions, attenuates the immune response and increases cancer cell locomotion into the modified region[5]. Gillies et al reported that chronic alkalinization with systemic buffers such as bicarbonate inhibited the formation of spontaneous lung metastases[11], which verifies the important role of the acidic pH_e played in tumor metastases. Due to the acidic extracellular fluid is a universal characteristic of solid tumors regardless of tumor genotype and phenotype, non-invasively imaging tumoral acidity creates a new opportunity to visualize metastases with high target to background (T/B) ratio.

Compared to the clinically used imaging modalities such as magnetic resonance imaging (MRI), positron emission tomography (PET) and computerized tomography (CT), optical imaging is still in its childhood. However, optical imaging holds

the promise for tumor diagnosis because of its superior sensitivity (pM–nM), fast-acquisition rate (ms–s), no ionizing radiation and low-running cost[11]. Among the optical imaging technologies, near-infrared (NIR) fluorescence imaging shows the advantage for *in vivo* imaging because absorbance and autofluorescence from endogenous molecules are low in the NIR wavelength (650–900 nm) range and NIR light can penetrate deeper tissue and generate images with improved sensitivity and spatial resolution[12]. For example, the NIR fluorescence probes successfully visualized the brain tumor non-invasively by penetrating the skull in small animal model[13, 14].

Due to the small volume and sporadic distribution of metastases, high T/B ratio is prerequisite to detect the metastases accurately and timely. Conventional targeting probes image neoplastic tissues by recognizing the tumor associated receptors. Even these receptor targeting probes have proven clinically useful[15], their capability to image primary tumors or metastases with diameter less than 1.0 cm is limited because the non-specific accumulation of the probe with "always on" fluorescence in surrounding normal tissues attenuates the T/B signal ratio. Therefore, responsive probes with signal that can be activated under tumor associated pathological condition will greatly increase T/B ratio and visualize metastases with high sensitivity. Actually, different types of responsive NIR fluorescence probes have been developed to monitor the tumor associated physiological evens such as over-expressed protease[16, 17], apoptosis [18] and hypoxia[19]. Even though numerous pH responsive NIR fluorescence probes have been developed[20-22], very a few of them successfully visualize metastases *in vivo* due to the poor biocompatibility, unmatched responsive pH range and unsatisfactory T/B ratio. To address these challenges, we developed a NIR fluorescence nanoprobe (NP) **NP2** in which multiple copies of NIR fluorophores IR783 with high extinction coefficient, quantum yield and photochemical stability were conjugated on dextran via acid liable hydrazone bond. This NP not only demonstrated remarkable NIR fluorescence intensity enhancement in the physiologically acidic pHs, but also successfully visualized the pulmonary metastases with volume as small as 0.5 mm^3. This pH responsive NIR fluorescence NP holds the promise to timely detect the metastases and reduce the metastasis associated mortality.

2. Materials and Methods

2.1 Materials

All chemical reagents and solvents for the probe synthesis were analytical grade and purchased from Sigma-Aldrich unless otherwise specified. Dextran (20 kDa) was purchased from Duly biology (Nanjing, China). PEG^{2k}–NHS was purchased from JenKem Technology Co. Ltd (Beijing, China). Rhodamine-N-hydroxy-succinimide ester, fetal bovine serum, penicillin, streptomycin and cell culture medium were purchased from Invitrogen (Carlsbad, USA). Water used in the study was purified by a Millipore Milli-Q Synthesis water system (Billerica, MA). Human breast tumor cells MDA-MB-231 were obtained from American Type Culture Collection (Manassas, VA). Fetal bovine serum (FBS) and 0.25% (w/v) trypsin solution were purchased from Gibco (Tulsa, OK, USA).

2.2 Characterization

The molar ratios of dextran and PEG in control probe **NP1** without pH sensitivity and pH responsive probe **NP2** were quantified by integrating the characteristic peaks of dextran (3.3–2.2 ppm) and PEG (3.7 ppm) in ^1H NMR spectra (Varian Mercury400 spectrometer, USA). Sodium Dodecyl Sulfate-Polyacrylamide Gel Electrophoresis (SDS-PAGE) was used to determine the purity and test fluorescence enhancement of nanoprobes under acidic environment. Briefly, the NPs were first incubated in buffer solution with pH 5.5 for 2 h. The NP samples were then added into 30 μL treatment buffer [100 mM Tris, pH 6.8, 2% (w/v) SDS, 12% (v/v) glycerol, 0.01% (w/v) bromphenol blue] and loaded on a 5% stacking gel, set upon a 10% resolving gel. After electrophoresis under a voltage of 70 V for 2 h, NIR fluorescent images of the resolved SDS-PAGE gels were acquired in Perkin Elmer Maestro™ small animal imaging system equipped with a 710–760 nm excitation filter and an 800 nm emission band pass filter set (FOV = 12.8 cm，f/stop = 4, bin = 2 × 2, exposure time = 1000 ms). Measurements of particle size and zeta potential of the NPs were performed by a Malvern Zetasizer (Malvern Instruments Inc., USA) dynamic light scattering instrument (DLS). A 2.0 mg/mL solution of bovine serum albumin (BSA) in distilled water was used for the instrument calibration. Samples for particle size measurements were diluted to 100 μg/mL with PBS (pH 7.4). The hydrodynamic radius and the size distribution patterns were calculated with the regularization algorithm. For zeta potential measurement, NPs were diluted to 200 μg/mL with 10 mM NaCl solution. The instrument was calibrated by commercial available standard solution with a Zeta potential of -50 mV. Each sample for particle size and zeta potential determination was filtrated through a 0.45 μm filter before measurements.

2.3 Photospectroscopic Studies

Stoke solutions of probes were prepared by dissolving **NP1** and **NP2** in 0.5 mL anhydrous DMF with a final concentration of 1.0 mg/mL. The working solutions for the spectroscopic measurement were prepared by diluting the stock solution into buffer solution with a concentration of 10 μg/mL. pH-dependent absorption spectra were recorded on a HIMADZU UV-2550 spectrophotometer in a quartz cuvette (10 × 10 mm) at 25 °C. Spectra was collected in the wavelength range of 450 to 950 nm at selected time points after incubation of NP under pH 5.5. pH-dependent emission spectra were collected on SHIMAZDU RF-5301PC spectrofluorophotometer in a quartz cuvette (10 × 10 mm) at 25 °C.

For the *in vitro* NIR fluorescence imaging studies, the stock solution of NP were diluted 100 times to buffers including 1X PBS (pH 7.4), 10 mM MES (pH 6.5) and 10 mM MES (pH 5.5) respectively with a final concentration of 10 μg/mL. The resulting working solution of NP was added to 96-well plate with a total volume of 100 μL in each well. The plate was incubated at 37 °C for 24 h and imaged under a Maestro™ small animal imaging system equipped with a 710–760 nm excitation filter and

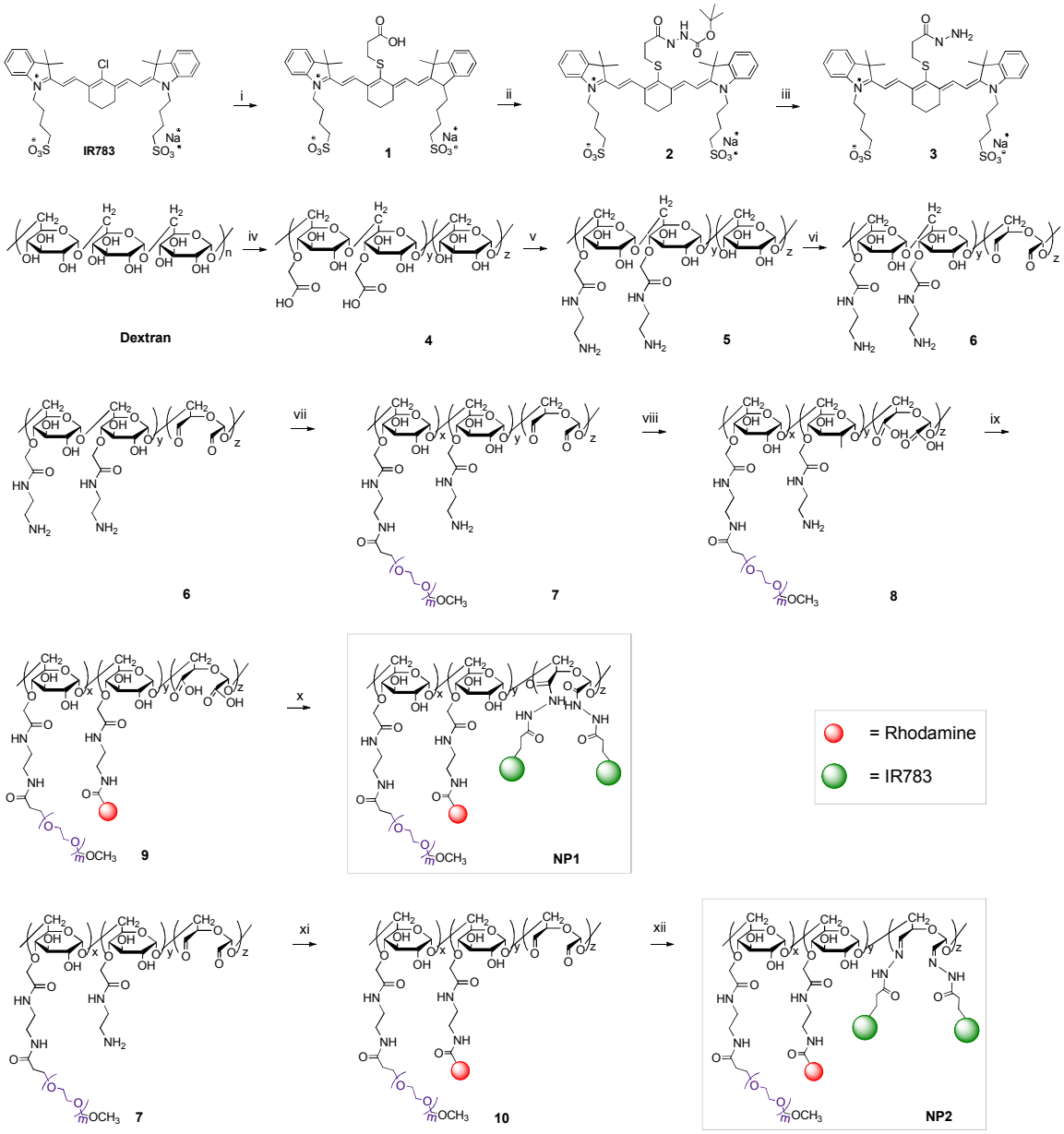

Figure 1. Synthesis of pH responsive nanoprobe **NP2** and control nanoprobe **NP1** without pH sensitivity. (i) $HS(CH_2)_2COOH$/DMF/TEA; (ii) Boc-Carbazate/EDC/HOBT; (iii) CF_3COOH/DCM; (iv) $ClCH_2COONa$/NaOH; (v) $NH_2(CH_2)_2NH_2$/EEDQ; (vi) $NaIO_4$; (vii) PEG^{2k}-NHS, pH 8.3; (vii) Br_2; (ix) rho-NHS, pH 8.3; (x) DMF/EDC/HOBT; (xi) Rho-NHS, pH 8.3; (xii) MES, pH 4.7.

an 800 nm longpass emission filter set (FOV = 12.8 cm，f/stop = 4, bin = 2×2, exposure time = 1000 ms).

2.4 Development of Metastasis Models

The development of mouse models bearing pulmonary metastases was performed according to a previously published method[23]. Human breast tumor cells MDA-MB-231 were cultured in DMEM (Life Technologies Bethesda Research Laboratories) supplemented with 10% fetal bovine serum (FBS; Atlanta Biologicals) at 37 °C in 5 % CO_2. Before injection, MDA-MB-231 cells were harvested with 1.0 mM EDTA in PBS, washed three times with serum-free DMEM and re-suspended in PBS with a cell density of 1×10^7 cells/mL. Male athymic nude mice (4–6 weeks) were intravenously injected with 1×10^6 MDA-MB-231 cells. All procedures were conducted under an approved protocol according to guidelines specified by the ethics committee of Fudan University (Shanghai, China).

2.5 *In Vivo* Optical Imaging Studies.

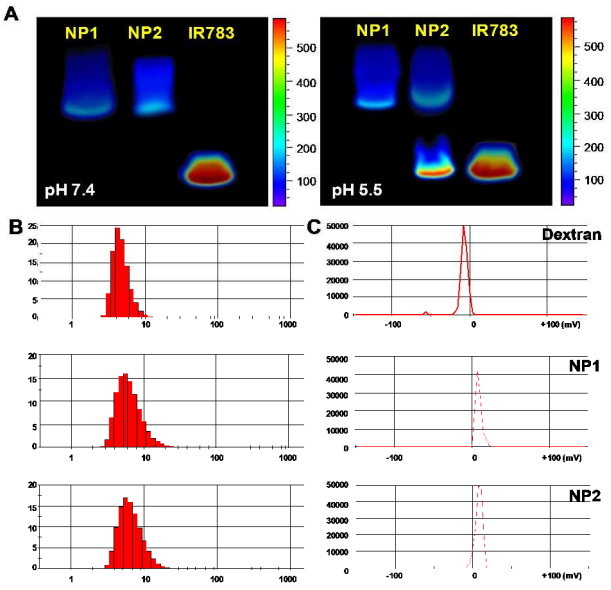

Figure 2. Characterization of the nanoprobes. (A) Color-coded (C.C.) NIR fluorescence images of resolved SDS-PAGE after loading NPs (30 μg per well) and free fluorophore IR783 (1.0 μg per well). Hydrodynamic size distribution (B) and Zeta potentials (C) of NPs measured by dynamic light scattering (DLS). The average hydrodynamic diameters of Dextran, **NP1** and **NP2** were measured as 4.8, 7.5 and 8.0 nm. The zeta potentials of above compounds were determined as -6.5, +8.7 and + 8.0 mV.

Table 1. Photophysical parameters of the NPs

Nanoprobe	d (nm)[a]	PDI [a]	ξ[a]	*Dex/PEG/Rho/IR783*[b]
Dextran	4.8	0.302	-6.5	1/0/0/0
NP1	7.5	0.271	+8.7	1/5.3/1.2/9.4
NP2	8.0	0.317	+8.0	1/5.6/1.3/9.7

[a]Diameters (d), polydispersity index (PDI), and zeta potentials (ζ) of the NPs were measured by dynamic light scattering (DLS) under pH 7.4; b Molar ratios of Dex/PEG/rhodamine/IR783 in the of the NPs.

NP was injected into the tail vein of the metastases bearing mice with a dose of 300 μg/mouse. At selected time post injection, the mice were anesthetized with 10 % chloral hydrate via intraperitoneal injection and imaged using a Maestro™ small animal imaging system equipped with a 710–760 nm excitation band pass filter and an 800 nm longpass emission filter. Images were acquired with the following parameters: exposure time: 1500 ms, FOV = 12.8 cm, f/stop = 4, Bin = high resolution. At the end of *in vivo* imaging, the mice were sacrificed and perfused with saline and 4% paraformaldehyde (PFA) in succession via heart to douche blood and pre-fix the mouse. Then tracheas of the mice were separated from the surrounding connective tissue and the catheters were inserted into lung and injected 0.6% agarose. The inflated lung and main organs including heart, liver, kidney, spleen, brain and muscle were carefully isolated and imaged with an exposure time of 1500 ms. The microscopic fluorescence intensities in healthy lungs and tumor bearing lungs were quantified by ImageJ (National Institutes of Health, Bethesda, MD) software.

2.6 Fluorescence Microscopic Imaging.

The agarose inflated lungs were excised and successively immersed in 4% PFA for 12 h, 15 % sucrose solution for 12 h and 30 % sucrose solution for 12 h. The lungs were then embedded in Tissue Tek O.C.T. compound (USA), frozen and sectioned coronally with a thickness of 5.0 μm using a cryotome Cryostat (Leica, CM 1900, Germany). To evaluate the targeting specificity of NP to pulmonary metastases, each two adjacent lung sections were stained by haematoxylin and eosin (H&E) staining and fluorescence staining of 4',6-diamidino-2-phenylindole (DAPI) respectively. The fluorescence microscopic images were collected using a Leica DMF4000B laser-scanning microscope (Leica Inc, Germany) equipped with a 10 × objective lens. The DAPI fluorescence was collected using an A4 filter tube (excitation: 360 ± 20 nm and emission: 470 ± 20 nm), the Rhodamine fluorescence was obtained using a N3 filter (excitation: 546 ± 6 nm and emission: 600 ± 20 nm). All the microscopic images were captured with an identical microscopic setting and processed by ImageJ software.

3. Results and Discussion

In the development of pH responsive NIR fluorescence probe **NP2** and control nanoprobe **NP1**, dextran was chosen as a platform due to its good biocompatibility[24], bio-degradability[25], convenience for modification[26] and the multiple particle sizes[27]. The heptamethine cyanine derivative IR783 was selected as NIR fluorophore because of its high extinction coefficient and quantum yield, optimal emission wavelength and good photochemical stability[28, 29]. IR783s were labeled in D-glucopyranosyl unit of dextran via pH sensitive hydrazone bond. The extra-close proximity of two IR783s and the multiple copies of such units will efficiently "silence" the fluorescence of the NPs via nonradioactive decay by forming intra/inter-unit fluorophore-aggregates in normal tissues[30]. Cleavage of the hydrazone bonds in acidic tumor microenvironment will diminish the distance-correlated fluorescence quenching and therefore result in the activation of NIR fluorescence. Functionalization of PEG on dextran benefits to improve the biocompatibility of the NPs[31]. Since NIR fluorophore cannot be excited well in excised tissues under fluorescent microscope, rhodamine was conjugated on the dextran to track the NPs under fluorescence microscope.

The synthesis of the NPs is demonstrated in Figure 1. A solution of IR783 (400 mg, 0.46 mmol), 3-mercaptopropionic acid (56 μL, 0.64 mmol) and triethylamine (88 μL, 0.64 mmol) in 6.0 mL anhydrous DMF were stirred at room temperature for 15 h. The solution was then dropped into an ice-cold methyl ether and purified by flash column chromatography (5:1, DCM: MeOH) to give compound **1**. EDC-HCl (60 mg, 0.31 mmol) and HOBT (50 mg, 0.37 mmol) were added to a solution of **1** (250 mg, 0.31 mmol) in ice cold anhydrous DMF (5.0 mL). Tert-butylcarbazate (34.5 mg, 0.26 mmol) was then added and the mixture was stirred at r.t. for overnight. After dropping above mixture into ice-cold diethyl ether, the precipitate was purified by flash column chromatography (5:1, DCM: MeOH) to afford compound **2**. **2** (30 mg, 0.03 mmol) was deprotected in a mixture of DCM and trifluoroacetic acid (4:1) to give compound **3** as

deep green powder. On the other hand, sodium chloroacetate

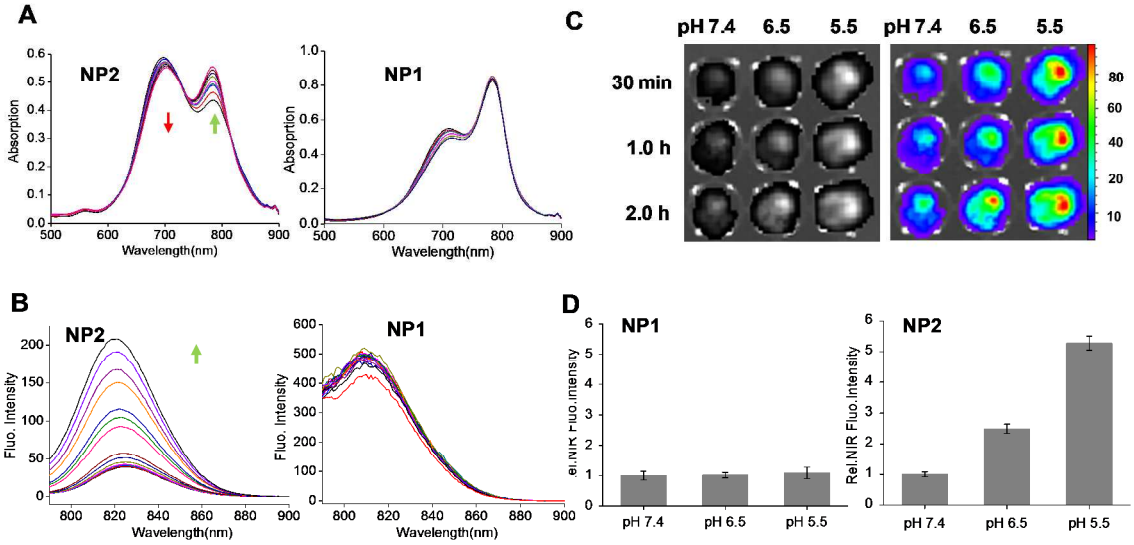

Figure 3. NP2 sensing physiologically acidic pH via remarkable NIR fluorescence enhancement. Time-dependent absorbance (A) and emission (B) of NPs (10 μg/mL) at pH 5.5. The NPs were excited at 770 nm. (C) NIR fluorescence images of **NP2** after incubation at pH 7.4, 6.5 and 5.5 for 0.5, 1.0 and 2.0 h in 96-well plates (10 μg/mL). (D) NIR fluorescence intensities of NPs (10 μg/mL) determined at 2 h post-incubation in buffered solutions with pH 7.4, 6.5 and 5.5.

(503 mg, 4.3 mmol) was added into a solution of dextran (MW: 20 kDa) in 6.0 M ice-cold NaOH. The mixture was stirred at 60 °C for 50 min and dropwise added into MeOH to give compound **4** as a white precipitate. The mixture of **4** (200 mg, 9.50 μmol) and EEDQ (320 mg, 1.29 mmol) in water solution was added dropwise into 0.41 mL ethylenediamine and the mixture was allowed to stir at r.t. for 4 h. After precipitation in the methanol, compound **5** was collected. The mixture of **5** (200 mg, 9.30 μmol) and sodium periodate (0.09 g, 0.43 mmol) in water solution was allowed to stir at r.t. for 24 h. At the end of reaction, 44 μL 2-(2-hydroxyethoxy) ethanol was added to quench the reaction. The product **6** was purified by using centrifugal filter (MW 3,000 cut off). Treatment of **6** (100 mg, 4.76 μmol) with PEG^{2K}-NHS ester (47.5 mg, 0.02 mmol) in 0.1 M HEPES buffer (pH 8.5) gave compound **7** after purification. 0.36 mL liquid bromine was added into a water solution of **7** (200 mg, 6.5 μmol). After stirring at r.t. in dark for 18 h, the product was purified to offer compound **8**. Rhodamine-NHS ester (3.4 mg, 6.4 μmol) in anhydrous DMF was added into **8** (100 mg, 2.9 μmol) in 0.1 M HEPES buffer solution (pH 8.5). After stirring at r.t. for 2 h, the product was purified to obtain compound **9**. EDC-HCl (12.1 mg, 0.06 mmol) and HOBT (8.5 mg, 0.06 mmol) in 0.5 mL DMF was added to **9** (63 mg, 1.8 μmol) in 500 μL DMF. After reaction at 0 °C for 5 min, the solution was added with compound **3** (78.6 mg, 0.09 mmol) in 0.5 mL DMF. The mixture was stirred at r.t. for 16 h and purified to give control nanoprobe **NP1** with a yield of 70% (based on dextran). To prepare the pH responsive NP, **7** was labeled with rhodamine to give compound **10**. **10** (50 mg, 1.6 μmol) dissolved in 1.0 M MES buffered solution with pH 4.7 was treated with **3** (62.3 mg, 0.07 mmol) in DMF. The mixture was stirred under pH 4.7 for overnight to obtain aiming nanoprobe **NP2** which was further purified by ultrafiltration filter (MW 10000 cut off) with a yield of 77.4 % (based on dextran).

The purity of the NPs was studied by the fluorescence images of the resolved SDS-PAGE (Figure 2A). All the purified NPs migrated as a single band, which implies their molecular distribution in a relatively narrow range. Notably, compared to the migration band of free fluorophore IR783, the fluorescence intensity of the NP bands was significantly weaker, which can be explained to the self-quenching of the NIR fluorophores labeled in NP via intramolecular nonradioactive decay. After incubation under pH 5.5 for 24 h, the band of free IR783 was appeared below the band of **NP2** due to the cleavage of the acid liable bond. Above data verified the purity of the NPs and the successful conjugation of NIR fluorophores on the NPs. The molar ratio of Dextran/PEG/IR783 in **NP1** and **NP2** were determined as 1/5.3/9.4 and 1/5.6/9.7 according to the method described previously[32] (Table 1). Additionally, averagely 1.2−1.3 rhodamine fluorophores were labeled on the NPs.

As shown in Table 1 and Figure 2B, **NP1** and **NP2** demonstrated higher hydrodynamic diameters than that of unconjugated dextran. The average hydrodynamic diameters of dextran, **NP1** and **NP2** were determined as 4.8, 7.5 and 8.0 nm respectively. After the multiple modifications, the positive charges of **NP1** and **NP2** (+8.7 and +8.0 mV) were determined in contrast to the negative charge of the unconjugated dextran (-6.5 mV). Compared to the value of free dextran without any modifications, the increased particle size of **NP1** and **NP2** can be explained by the modification of PEG with extended linear structure. Additionally, the increased positive charge in the NPs can be attributed to the functionalization of the primary amines that could be protonated under the neutral pHs.

Time dependent absorption and emission spectra of the NPs were measured at pH 5.5 that mimic the acidic environment (Fig. 3 A–B). As shown in Fig. 3A, there are two absorption peaks at 670 and 783 nm that can be assigned to the H-type IR783 aggregate and free IR783 monomer. Notably, under an acidic

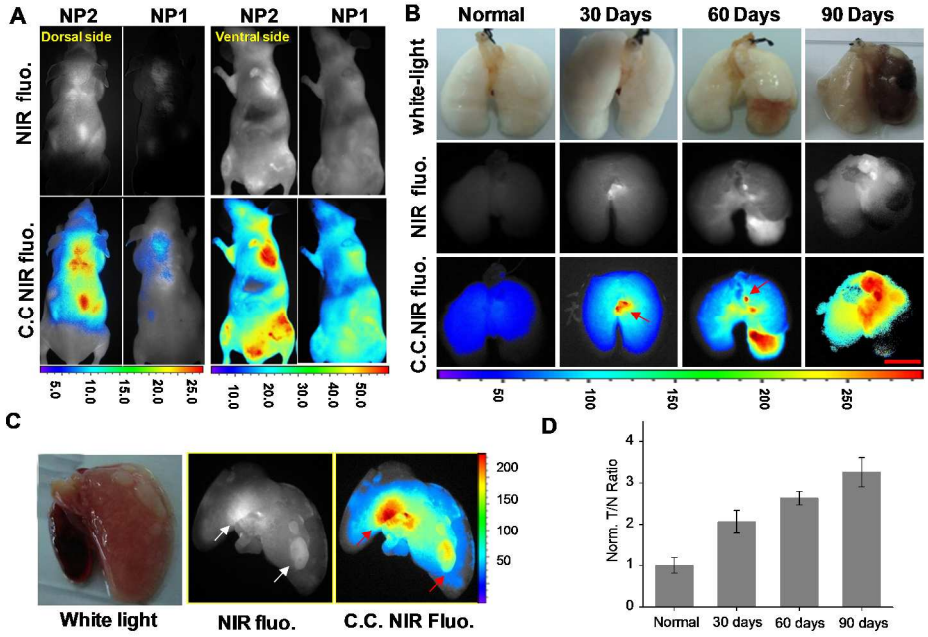

Figure 4. NP2 visualized pulmonary metastases by sensing acidic environment. (A) *In vivo* NIR fluorescence images of mouse bearing metastases with ventral and dorsal positions at 24 h PI of NP (300 μg/mouse). (B) Representative white light, NIR fluorescence and color coded (C.C.) fluorescence images of mouse lung at 24 h PI of **NP2**. The lungs were excised from mice at 0, 30, 60 and 90 days post tail vein injection of cancer cells. Scale bar: 1.0 mm and the arrows indicate the smallest metastases. (C) Enlarged white-light and NIR fluorescence images of metastasized lung (90 days inoculation) at 24 h PI of **NP2**. Arrows point to the metastases. (D) Mean T/B signal ratio of mice (n = 4) at 30, 60 and 90 days post inoculation of **NP2**.

pH, a consistent increase in monomer absorbance with a concomitant decrease in aggregate absorbance was observed in the absorption spectrum of **NP2**. The absorbance ratio between IR783 aggregate and monomer (A670/A785) decreased from 1.38 to 0.98, indicating the de-association of the aggregates under acidic pHs[33-35]. For the control probe **NP1**, both the absorbance of monomer and aggregate barely changed under neutral or acidic pHs (Figure 3A). Fluorospectroscopic studies demonstrated that NIR fluorescence intensity of **NP2** maximally increased 7.7 times after 2.0 h incubation under pH 5.5 (Figure 3B). In contrast, the fluorescence of **NP1** kept quenching in the first 2.0 h post incubation. The pH dependent fluorescence enhancement of NPs was further verified by NIR fluorescence imaging studies in 96-well plate. Remarkable fluorescence enhancements were observed for **NP2** but not **NP1** under acidic environment. Averagely, the fluorescence intensities of **NP2** under pH 6.5 and 5.5 were determined as 2.5 and 5.3 folds higher than that measured under pH 7.4 after incubating for 2.0 h.

The capability of the pH responsive NP to visualize metastases was conducted in mouse models bearing human breast MDA-MB-231 metastases in the lung. After tail vein injection of the MDA-MB-231 cancer cells, the development of pulmonary metastases was monitored by *in vivo* and *ex vivo* NIR fluorescence imaging. *In vivo* NIR fluorescence imaging showed the remarkable NIR fluorescence signal in the chest area of the metastasized mice (Figure 4A). In contrast, no obvious signal was detected after the administration of **NP1**. *Ex vivo* NIR fluorescence images of mouse lung verified the development of metastases after intravenous injection of **NP2**. The metastases volume increased with the time after cell injection. The average volume of the metastases was initially determined as 0.5 mm^3 at 30 days post-injection (PI), but increased to 2.0 mm^3 at 60 days and 28 mm^3 at 90 days PI (Figure 4B). **NP2** clearly visualized the metastases with T/B ratio as high as 3.2 at 24 h PI (Figure 4C). Figure 4D demonstrated the mean NIR fluorescence

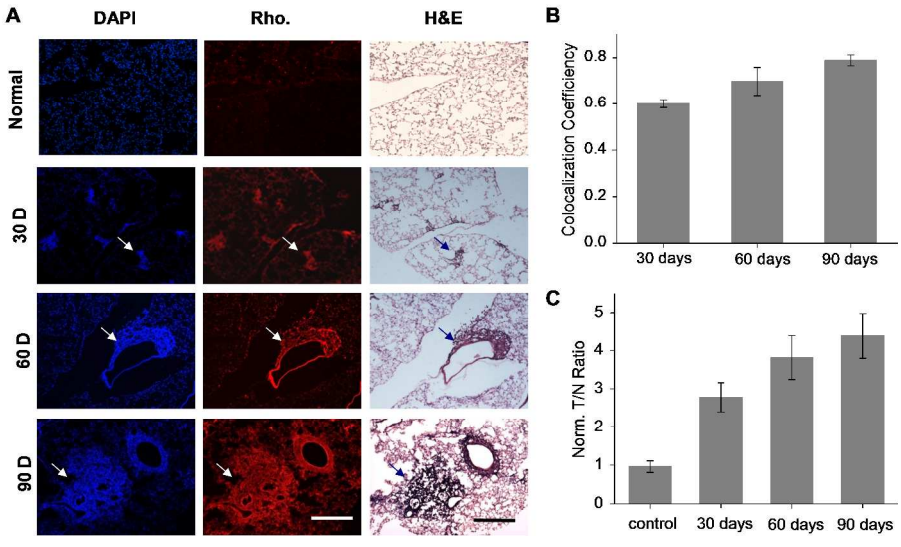

Figure 5. NP2 visualized pulmonary metastases with high T/B ratio. (A) Representative fluorescence microscopic images of mouse lung sections at 24 h PI of **NP2** (300 μg/mouse). The lungs were excised at 0, 30, 60 and 90 days post inoculation of cancer cells. Rhodamine fluorescence of NP was displayed in red. H&E staining of lung sections with the same field of views verified the metastases. Scale bar: 500 μm. (B) High colocalization coefficients between NP and neoplastic tissues indicated by H&E staining were observed in mice at 30, 60 and 90 days after cancer cell inoculation. The mice were imaged at 24 h PI of **NP2**. (C) T/B ratios of pulmonary metastases at 24 h PI of **NP2**. The values were quantified from 24 randomly selected images from 4 mice (n = 4).

intensity ratio between the metastasized mouse lungs and normal lung. Interestingly, **NP2** exhibited high fluorescence in kidney but low signal intensities in liver and other main organs. This phenomenon could be explained by the weak acidic condition of renal distal convoluted tubules and collecting duct[36]. Besides the signal activation in acidic extracellular fluid, **NP2** could also be internalized by the cancer cells and delivered into acidic organelles such as lysosomes followed the fluorescence signal activation[37, 38]. Actually the high T/B signal ratio of **NP2** may contributed from pH activated fluorescence enhancement in both the acidic extracellular fluid and the acidic organelles. Overall, *in vivo* NIR fluorescence imaging studies clearly revealed the capability of pH responsive NP to detect pulmonary metastases by sensing the acidic environment.

Figure 5 demonstrated the fluorescence microscopy imaging and histological H&E staining imaging of mouse lung sections at 24 h PI of **NP2**. Interestingly, **NP2** indentified the metastases with high targeting specificity with the evidence of the high colocalization coefficient between the rhodamine fluorescence of **NP2** and the neoplastic tissue indicated by H&E staining (Figure 5B). The capability of **NP2** to accurately delineate metastases can be interpreted by the enhanced permeability and retention (EPR) effect [39, 40] due to the prolonged circulation lifetime of NP and the increased permeability of tumor vasculatures. Quantification analysis showed that the T/B ratio of pulmonary metastases increased with the volume of the metastases after injection of **NP2** via *i.v.*. The T/B ratios were determined as 2.8 ± 0.3, 3.8 ± 0.4 and 4.4 ± 0.4 at 30, 60 and 90 days post cancer cell inoculation. This phenomenon can be interpreted by the increased vessel density and vasculature permeability with the development of metastasis.

4. Conclusions

In conclusion, we developed a pH response NIR fluorescence nanoprobe that demonstrated the capability to visualize metastases with high T/B ratio. Due to the high penetration depth of NIR fluorescence combined with the pH activated fluorescence as well as EPR effect of the nanoprobe, we successfully extended the application of the NIR fluorescence imaging from the detection of primary tumor to metastases with diameter as small as 0.5 mm^3 in volume. Considering the high sensitivity and T/B ratio, this pH responsive nanoprobe holds the promise to identify the scatteredly distributed metastases from surrounding normal tissues and provide the guidance of image-guided surgery.

Acknowledgements

This work was supported by the National Basic Research Program of China (973 Program, 2011CB910404, 2013CB932500), the National Natural Science Foundation of China (Nos. 81171384), New Century Excellent Talents in University Award, and the Shanghai Foundation for Development of Science and Technology (Nos. 13NM1400400, 12NM0501400).

Notes and references

[a] *Key Laboratory of Smart Drug Delivery, Ministry of Education, School of Pharmacy, Fudan University, 826 Zhangheng Rd., Shanghai 201203, China; E-mail: congli@fudan.edu.cn*

1. A. F. Chambers, A. C. Groom and I. C. MacDonald, *Nature reviews. Cancer*, 2002, **2**, 563-572.

2. B. Weigelt, J. L. Peterse and L. J. van 't Veer, *Nature reviews. Cancer*, 2005, **5**, 591-602.

3. S. Paget, *Cancer Metastasis Rev*, 1989, **8**, 98-101.

4. M. M. Mueller and N. E. Fusenig, *Nature reviews. Cancer*, 2004, **4**, 839-849.

5. B. A. Webb, M. Chimenti, M. P. Jacobson and D. L. Barber, *Nature reviews. Cancer*, 2011, **11**, 671-677.

6. R. van Sluis, Z. M. Bhujwalla, N. Raghunand, P. Ballesteros, J. Alvarez, S. Cerdan, J. P. Galons and R. J. Gillies, *Magn Reson Med*, 1999, **41**, 743-750.

7. J. W. Wojtkowiak, J. M. Rothberg, V. Kumar, K. J. Schramm, E. Haller, J. B. Proemsey, M. C. Lloyd, B. F. Sloane and R. J. Gillies, *Cancer research*, 2012, **72**, 3938-3947.

8. V. Estrella, T. Chen, M. Lloyd, J. Wojtkowiak, H. H. Cornnell, A. Ibrahim-Hashim, K. Bailey, Y. Balagurunathan, J. M. Rothberg, B. F. Sloane, J. Johnson, R. A. Gatenby and R. J. Gillies, *Cancer research*, 2013, **73**, 1524-1535.

9. R. A. Gatenby and R. J. Gillies, *Nature reviews. Cancer*, 2004, **4**, 891-899.

10. N. C. Denko, *Nature reviews. Cancer*, 2008, **8**, 705-713.

11. I. F. Robey, B. K. Baggett, N. D. Kirkpatrick, D. J. Roe, J. Dosescu, B. F. Sloane, A. I. Hashim, D. L. Morse, N. Raghunand, R. A. Gatenby and R. J. Gillies, *Cancer research*, 2009, **69**, 2260-2268.

12. L. Fass, *Molecular Oncology*, 2008, **2**, 115 - 152.

13. H. Yan, J. Wang, P. Yi, H. Lei, C. Zhan, C. Xie, L. Feng, J. Qian, J. Zhu, W. Lu and C. Li, *Chemical Communications*, 2011, **47**, 8130-8132.

14. H. Yan, L. Wang, J. Wang, X. Weng, H. Lei, X. Wang, L. Jiang, J. Zhu, W. Lu and X. Wei, *ACS nano*, 2011, **6**, 410-420.

15. S. Luo, E. Zhang, Y. Su, T. Cheng and C. Shi, *Biomaterials*, 2011, **32**, 7127-7138.

16. C. J. Mu, D. A. Lavan, R. S. Langer and B. R. Zetter, *ACS nano*, 2010, **4**, 1511-1520.

17. K. Welser, R. Adsley, B. M. Moore, W. C. Chan and J. W. Aylott, *Analyst*, 2011, **136**, 29-41.

18. K. Kim, M. Lee, H. Park, J. H. Kim, S. Kim, H. Chung, K. Choi, I. S. Kim, B. L. Seong and I. C. Kwon, *J Am Chem Soc*, 2006, **128**, 3490-3491.

19. K. Kiyose, K. Hanaoka, D. Oushiki, T. Nakamura, M. Kajimura, M. Suematsu, H. Nishimatsu, T. Yamane, T. Terai, Y. Hirata and T. Nagano, *J Am Chem Soc*, 2010, **132**, 15846-15848.

20. S. A. Hilderbrand and R. Weissleder, *Chemical communications*, 2007, 2747-2749.

21. E. M. Barnett, X. Zhang, D. Maxwell, Q. Chang and D. Piwnica-Worms, *Proc Natl Acad Sci U S A*, 2009, **106**, 9391-9396.

22. Y. Urano, D. Asanuma, Y. Hama, Y. Koyama, T. Barrett, M. Kamiya, T. Nagano, T. Watanabe, A. Hasegawa, P. L. Choyke and H. Kobayashi, *Nat Med*, 2009, **15**, 104-109.

23. Y. Zhou, G. Shao and S. Liu, *Theranostics*, 2012, **2**, 577-588.

24. M. Naessens, A. Cerdobbel, W. Soetaert and E. J. Vandamme, *Journal of Chemical Technology & Biotechnology*, 2005, **80**, 845-860.

25. J. S. Roberts and S. L. Bratton, *Drugs*, 1998, **55**, 621-630.

26. M. Sokolsky-Papkov, A. J. Domb and J. Golenser, *Biomacromolecules*, 2006, **7**, 1529-1535.

27. M. A. Casadei, G. Pitarresi, R. Calabrese, P. Paolicelli and G. Giammona, *Biomacromolecules*, 2008, **9**, 43-49.

28. S. A. Hilderbrand, K. A. Kelly, R. Weissleder and C. H. Tung, *Bioconjug Chem*, 2005, **16**, 1275-1281.

29. C. Li, T. R. Greenwood, Z. M. Bhujwalla and K. Glunde, *Org Lett*, 2006, **8**, 3623-3626.

30. R. Khairutdinov and N. Serpone, *The Journal of Physical Chemistry B*, 1997, **101**, 2602-2610.

31. F. M. Veronese and G. Pasut, *Drug Discov Today*, 2005, **10**, 1451-1458.

32. C. Li, P. T. Winnard, T. Takagi, D. Artemov and Z. M. Bhujwalla, *Journal of the American Chemical Society*, 2006, **128**, 15072-15073.

33. L. Wang, X. Zhu, C. Xie, N. Ding, X. Weng, W. Lu, X. Wei and C. Li, *Chemical communications*, 2012, **48**, 11677-11679.

34. C. Li, K. Li, H. Yan, G. Li, J. Xia and X. Wei, *Chemical communications*, 2010, **46**, 1326-1328.

35. G. Huang, Z. Si, S. Yang, C. Li and D. Xing, *Journal of Materials Chemistry*, 2012, **22**, 22575-22581.

36. J. J. Ackerman, M. Lowry, G. K. Radda, B. D. Ross and G. G. Wong, *J Physiol*, 1981, **319**, 65-79.

37. Z. Li, Y. Song, Y. Yang, L. Yang, X. Huang, J. Han and S. Han, *Chemical Science*, 2012, **3**, 2941-2948.

38. X. Wu, Y. Tian, M. Yu, J. Han and S. Han, *Biomaterials Science*, 2014, **2**, 972-979.

39. H. Maeda, *Bioconjug Chem*, 2010, **21**, 797-802.

40. V. Torchilin, *Adv Drug Deliv Rev*, 2011, **63**, 131-135.

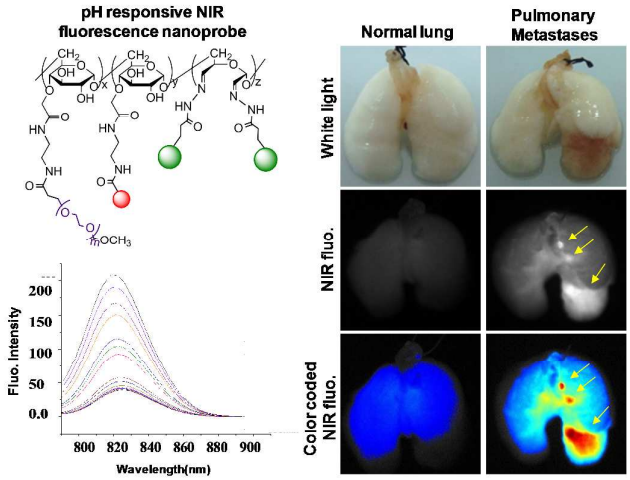

A pH responsive near-infrared fluorescence nanoprobe was developed and visualized pulmonary metastases in mouse model with volume as small as 0.5 mm^3 by sensing the acidic tumor microenvironment.